Applied Physics A (2019)125:816
https://doi.org/10.1007/s00339-019-3118-3

Applied Physics A
Materials Science & Processing

Synthesis and evaluation of the structural, microstructural, optical and magnetic properties of $Zn_{1-x}Co_xO$ thin films grown onto glass substrate by ultrasonic spray pyrolysis

Sabrina Roguai[1,2] · Abdelkader Djelloul[1,2]

Received: 31 July 2019 / Accepted: 29 October 2019

Abstract
Ultrasound pyrolysis spray technique is used to prepare single-phase thin films of $Zn_{1-x}Co_xO$ ($x = 0$–22 at.%). The hexagonal wurtzite structure of the films is confirmed by X-ray diffraction with an average crystallite size estimated in the range of 18–30 nm. The compound structure and stoichiometry of the films are further characterized by energy-dispersive spectroscopy (EDAX). The spectrum analysis agreement great chords between the expected and measured Co atomic content in the films indicating an effective doping. The results also reveal a high solubility of Co into ZnO solid solution at about 14 at.%. For the optical proprieties, the bandgap energy decreases due to the presence of high concentrations of localized states in the thin films. The photoluminescence spectra of all the samples exhibited a broad emission in the visible range. In addition, the magnetic properties of $Zn_{1-x}Co_xO$ thin films are found to be strongly influenced by Co doping.

1 Introduction

Zinc oxide semiconductors have demonstrated extraordinary properties in recent years due to their extensive applications particularly in the field of spintronics. ZnO is a semiconductor with a large bandgap ($E_g = 3.31$ eV) and large exciton binding energy ~ 60 meV at room temperature [1]. In a hand, these properties make them more interesting for optoelectronic applications [2]. On the other hand, the nonstoichiometric structure of ZnO and the intrinsic structural defects such as oxygen vacancies (V_O) and zinc interstitial (Zn_i) improves the transparent conductive properties [3, 4]

Recently, transition metal-doped semiconductors have been at the core of various research reviews due to their exceptional optical properties and the promising potential applications in the optoelectronic medium [5-8]. The doping of ZnO by transition metals, in particular by cobalt, draws the attention of many researches. Cobalt (Co) doping is greater because of similar ionic radii (0.058 nm) to that of Zn (0.060 nm), and its powered magnetic moment compared to other 3*d* metals ($\mu_{Co} = 1.8\ \mu_B$) [9]. This type of doping is known as diluted magnetic semiconductor (DMS) because ZnO provides ferromagnetic properties at room temperature [10].

Thin layers of Co-doped ZnO were synthesized by the use of different evaporation techniques [11-14]. In thin film, doping ZnO with Co^{2+} improves optical absorption and decreases the band gap which is assigned to the *sp–d* spin exchange interaction [15-17]. Note that the defect environment can be distort when Co dopant atom substitutes a Zn atom. Along these lines, it is interesting to study the influence of this doping on the optical properties of Co-doped ZnO.

Many studies listed in the literature, on the elaboration of thin layers of ZnO, $Zn_{1-x}Co_xO$ with different techniques under different experimental conditions, produce in the formation of single-phase films, with different properties.

Ivill et al. [18] observed the plane, i.e., (0 0 2) of ZnO along with the secondary phase of (0 0 4) plane of Co ions. They observed paramagnetic behavior for 0–15 at.% of cobalt, for higher (>30 at.%) cobalt, they noticed ferromagnetic behavior, which was due to intrinsic defects and a large amount of Co^{+2} within the ZnO lattice. Tarwal et al. [19] prepared Co-doped ZnO films with 0–20 at.% doping, confirmed the polycrystalline nature of the films with (0 0 2)

✉ Sabrina Roguai
rog.sabrina@yahoo.fr

[1] LASPI2A Laboratoire des Structures, Propriétés et Interactions Inter Atomiques, Université Abbes Laghrour, 40000 Khenchela, Algeria

[2] Science of Matter, Abbes Laghrour University, Khenchela, Algeria

Published online: 07 November 2019

plane with flower-like morphology, and they also observed a reduction of band gap and transmittance with increases in the Co. PL measurements indicate only the emission in the visible region, which is caused by Co doping [20].

Some groups have observed room temperature ferromagnetism (RTFM) in cobalt-doped ZnO without any secondary phases or cobalt clusters [21, 22], in contrary to the reports on non-observation of RTFM [23, 24] or the observed ferromagnetism due to metallic cobalt clusters [25, 26]. Siddheswaran et al. [27] found that the ferromagnetic behaviour of films increases with 'Co' content. $Zn_{0.95}Co_{0.05}O$ thin film shows RTFM with saturation magnetic moment of $0.4\mu_B$/Co atom. The magnetic properties rely on intricate combination of transition metal dopants and material defects such as oxygen vacancies which are difficult to characterize [28].

The main goal of this study is to investigate the influence of Co doping on structural, optical and magnetic properties of pure and Co-doped ZnO thin films deposited by the ultrasound spray pyrolysis technique (USP).

2 Experimental

2.1 Film preparation

In this study, the ultrasonic pyrolysis spray technique was used to synthesize ZnO, $Zn_{1-x}Co_xO$ films. This technique has many advantages [29]. The solution utilized for the investigated films has the following composition: 0.01 M of zinc acetate [Zn $(CH_3COO)_2{\cdot}2H_2O$)] (Fulka 99.9%); 50 ml of deionized water (resistivity 18.2 MO cm); 20 ml CH_3OH (Merck 99.5%); 30 ml C_2H_5OH (Merck 99.5%) and cobalt nitrate hexahydrate 1–22% (Co, at. %) [Co $(NO_3)_2{\cdot}6H_2O$] has been used as the Co source. To settle the pH value to about 4.8, a little quantity of acetic acid is added, so as to prevent the evolution of hydroxides. Thin films were deposited onto microscope cover glass substrates ($30\times10\times1.2$ mm^3) at the temperature of 450 °C and the testimony time was fixed at 30 and 45 min. Details are listed in the works [29].

2.2 Characterization techniques

Structural properties were recorded using a high-resolution diffractometer (Rigaku Ultima IV powder) equipped with Cu–K_α radiation ($\lambda = 1.5418$ Å). The microstructure was analyzed utilizing scanning electron microscope (SEM) (FEI Quanta^{TM} 250 FEG). The SEM is equipped with an energy-dispersive X-ray spectroscopy (EDAX) detector with working distance of 10 mm, acceleration voltage ranging from 5 to 20 keV at two magnifications of 10,000 and 20,000 that were employed to quantify the composition of the films and to validate the doping efficiency. Genesis software was used for analysis of EDAX spectra. The secondary electron detector was used for imaging. Since the films were not conductive, silver paint contact and deceleration voltage method were used to decrease the charging effect and enhance the spatial resolution. The optical properties of thin films were estimated utilizing a Perkin Elmer UV–Vis–NIR (Lambda 19) spectrophotometer in the range 190–1800 nm. Photoluminescence measurements of prepared samples were examined using a Perkin Elmer (LS 45) fluorescence spectrometer with an excitation wavelength of 320 nm. Magnetic measurements were performed using EV-7 VSM vibrating sample magnetometer in magnetic field ≤ 20 kOe.

3 Results and discussion

3.1 Structure and microstructure analysis

Figure 1 reveals the X-ray spectra of pure and cobalt-doped ZnO. All spectra show the presence of hexagonal wurtzite structure of ZnO that is confirmed with (JCPDS card no. #00–036–1451). The peaks are broad and their relative intensity changes with Co content. The preferred orientation of the growth during deposition changes with Co doping level: along (002) for pure ZnO (101) for $x_{Co} = 0.01$, then again (002) for x_{Co} in the interval of 0.03–0.14, and finally to random orientations for higher Co content.

Table 1 presents the results of the phases examined qualitatively and quantitatively by the Rietveld method. The fit parameters are R_{wp} (%), weight profile R-factor; R_p (%), profile R-factor; R_e (%), expected R-factor; $S = R_{wp}/R_e$; and $\chi^2 = S^2$, goodness of fit. It can be observed that the size of crystallite varies within a narrow range of 18–30 nm, whereas the micro-strain changes considerably with Co content into the range of 0.131–0.289%.

The lattice parameter "a" increases with Co content while "c" seems not much affected, therefore, the volume of unit cell grows with increasing Co. However, the evolution of lattice parameters with Co content is more complex than expected. Four factors should be taken into consideration, as their effects occur concurrently:

1. According to Vegard's law, it is expected that the lattice parameters would slightly decrease with increasing Co content, Co ionic radius is smaller than that of Zn. In fact, in our case, it is slightly different, Zn^{2+} in tetrahedral coordination with an ionic radius of 0.060 nm will not be completely filled by Co^{2+} in tetrahedral coordination with an ($r_{Co}{}^{2+} = 0.058$ nm) but also with Co^{2+} in octahedral coordination with an $r = 0.065$ nm (low spin) or/and 0.075 nm (high spin) [30]. The substitution of Co into tetrahedral coordination was confirmed by transmittance measurements (see Sect. 3.2).

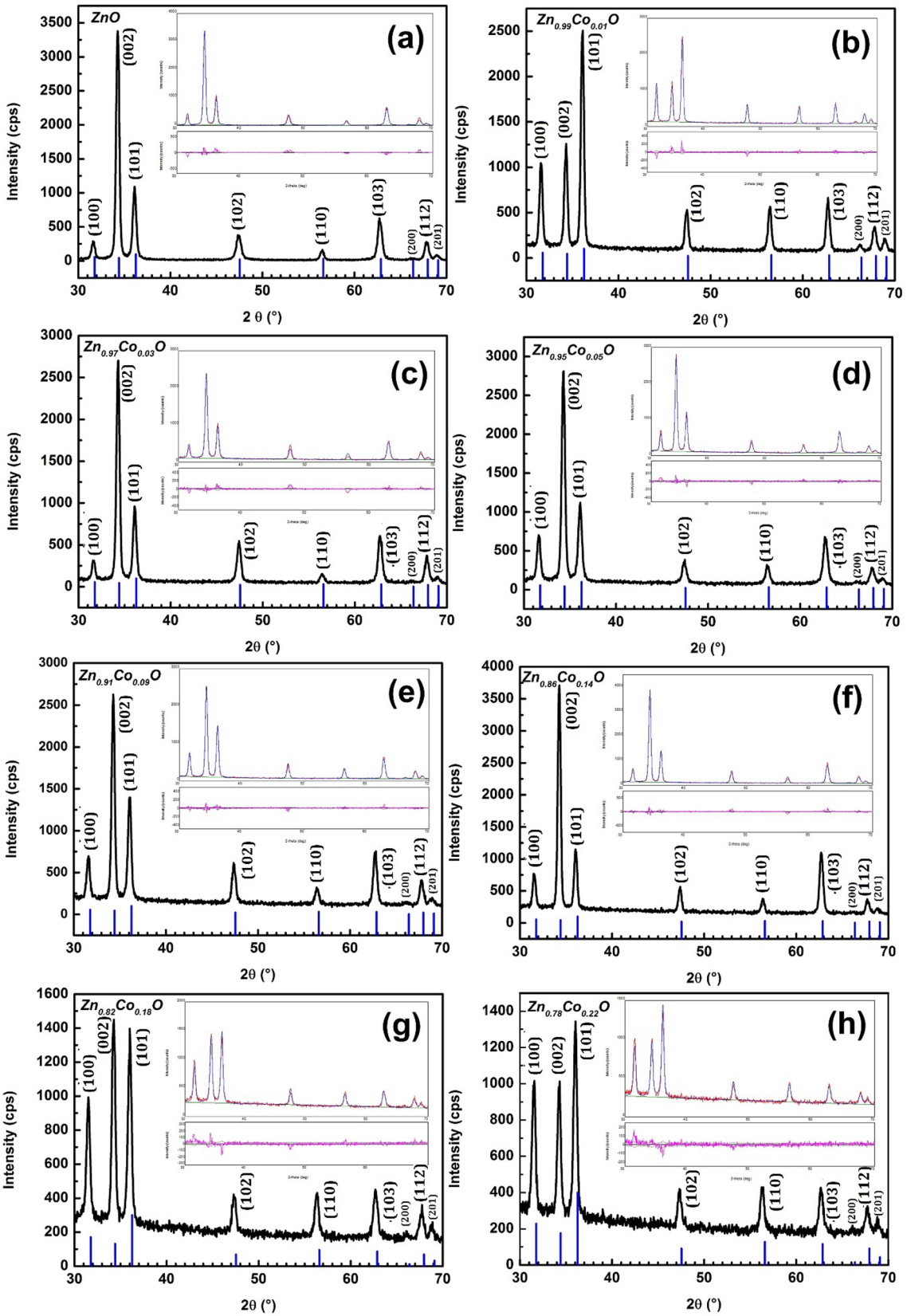

Fig. 1 XRD patterns of pure ZnO and Co-doped ZnO films. The inset shows the Rietveld refinements of $Zn_{1-x}Co_xO$ composition. Solid blue curve: calculated pattern; red solid line: experimental data; solid orange line (down): intensity difference

Table 1 X-ray diffraction Rietveld refinements results

Composition	Crystallite size (nm)	Microstrain (%)	Lattice parameters (Å)	*R*wp (%)	Refinements R_p (%)	Factors R_e (%)	*S*	χ^2
ZnO	25	0.266	$a=3.2542$ $c=5.2129$	16.87	11.84	8.93	1.71	2.92
$Zn_{0.99}Co_{0.01}O$	21	0.210	$a=3.2577$ $c=5.2124$	9.21	7.37	7.55	1.21	1.48
$Zn_{0.97}Co_{0.03}O$	35	0.230	$a=3.2594$ $c=5.2172$	8.23	6.28	5.40	1.52	2.32
$Zn_{0.95}Co_{0.05}O$	23	0.289	$a=3.2572$ $c=5.2162$	9.58	7.41	7.63	1.25	1.57
$Zn_{0.91}Co_{0.09}O$	22	0.131	$a=3.2613$ $c=5.2172$	8.55	6.64	6.76	1.26	1.59
$Zn_{0.86}Co_{0.14}O$	25	0.143	$a=3.2605$ $c=5.2148$	8.94	6.99	6.15	1.45	2.11
$Zn_{0.82}Co_{0.18}O$	18	0.147	$a=3.2689$ $c=5.2230$	8.40	6.72	6.18	1.36	1.85
$Zn_{0.78}Co_{0.22}O$	18	0.142	$a=3.2644$ $c=5.2167$	8.02	6.55	6.12	1.31	1.71

2. According to size effect in nanomaterials, it is expected that with decreasing in particle (crystallites) size, lattice contraction is expected [31].
3. The mismatch between the glass substrate and the deposited thin film (ZnO) induces some stress within ZnO and may causes some lattice distortion, thereby the lattice parameters may vary accordingly [32].
4. The effect of deposition temperature (450 °C) on the stoichiometry, which means that possible O and/or Zn vacancies can be created, as well as O can occupy even interstitial sites [33]. This will induce some anisotropic changes in the lattice parameters.
5. Some Zn or/and Co may occupy interstitial sites as well, and this will result an alteration in lattice parameters as well.

Data in Table 1 show small difference in lattice parameters with increase of Co-doping level due to the introduction of stress which leading to the shift in peak position caused by the comparable ionic radii of Zn^{2+} and Co^{2+}. The substitution of Zn^{2+} ions by Co^{2+} ions would not induce strong geometrical distortion in ZnO unit cell, as the ionic radii difference is ~ 3%. Therefore, Co^{2+} ions could easily form substitutional solid solution (SSS) with Zn^{2+} ions in ZnO crystal. Some Co^{2+} ions might also occupy structural point defects like vacancies formed during synthesis.

Figure 2 shows SEM images at two magnifications of 10,000 and 20,000. To study the effect of the Co doping, the SEM images are compared to those recorded of pure ZnO (Fig. 2a).

Co doping seems to preserve the emerging nanopetals perpendicular to the film surface which distinguish ZnO microstructure. However, unlike the XRD data, the size and the length of these nanopetals increase with Co doping mainly and reach 1 µm at 14 at.%. In addition, population of nanosize spherical features can be distinguished with sizes of 30–60 nm mainly for the doping range of 3–14 at. %.

The SEM images (Fig. 2c–f) reveal that uniform nanograins present at the film surface and can be described as nanorods (or nanowires) developed mainly in perpendicular directions, few nanorods are also developed horizontally. It can also be noted the presence of nanofillers in a pure ZnO film (Fig. 2a). These forms confirm the crystal structure of wurtzite ZnO which is in agreement with the XRD.

In a line with XRD data, for a doping rate of 18 at.% and 22 at.%, it is noticed a deterioration in the crystalline structure. The nanostructures change from large nanopetals to fine nanograins with reduced size below 100 nm.

The films have spherical nanograins in the wurtzite structure increasing in size with the doping rate. This observed regularity is due to the good adhesion of the substrate mainly depends on the parameter of the spray pyrolysis process such as the deposition temperature which has a very important factor that determines the energy difference between the spray solution and the film substrate. Usually, the diffusion of the species of vapor occurs several times before these stabilize. Due to the pyrolytic decomposition of the solution, different atomic rearrangements occur, resulting in a modification of the topographic characteristics of the sample. As well as changes in the surface mobility of the species in condensation during growth and nucleation can be defined as the extent of crystallinity of the film [19, 34].

Figure 3a shows an example of EDAX spectra obtained for Co–ZnO (18 at. %). The EDAX spectrum reveals the different constituents of the samples mainly O, Zn, and Co from the films but also Si and Ca peaks from soda lime glass.

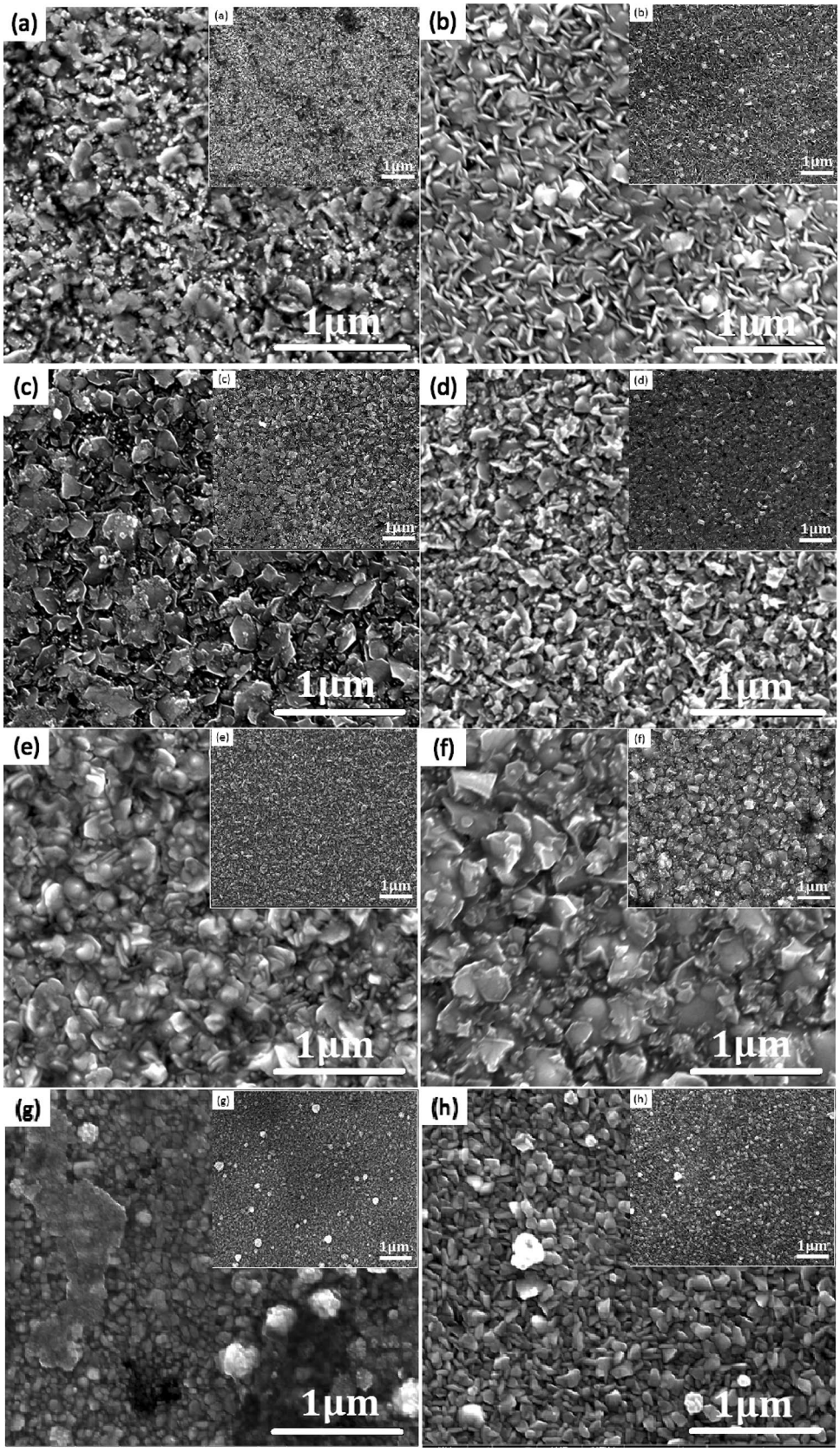

Fig. 2 SEM images of **a** pure ZnO film and **b–h** Co-doped $Zn_{1-x}Co_xO$ thin films. The images **b–h** correspond to the Co atomic content of 1%, 3%, 5%, 9%, 14%, 18% and 22%, respectively, and magnification of (× 10,000 and × 20,000)

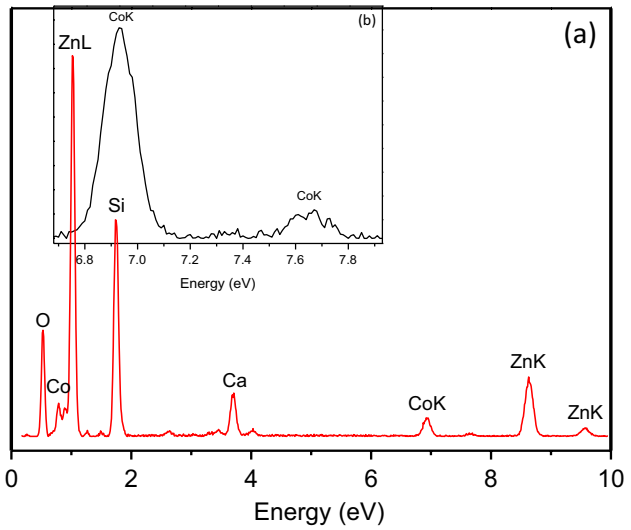

Fig. 3 **a** Example of EDAX spectra of Co-doped $Zn_{0.82}Co_{0.18}$ O showing the L-shell and K-shell of both Zn and Co, and **b** the EDAX peak of K-shell of Co

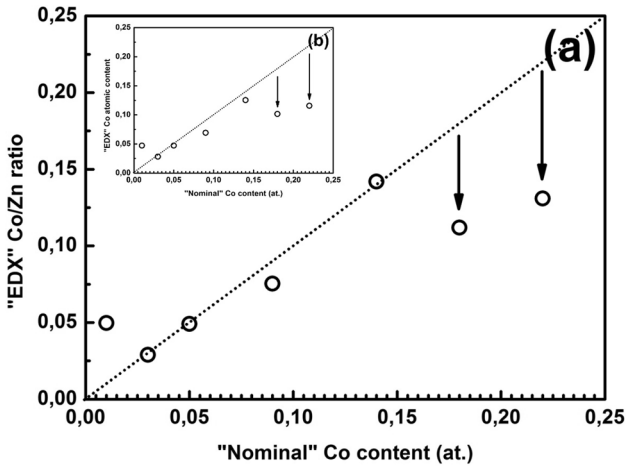

Fig. 4 **a** The measured Co/Zn atomic ratio and **b** the calculated Co atomic content (from EDAX analysis) plotted as function of the expected Co content/doping

It is noticed also that at 20 keV acceleration voltage, the L-shell and K-shell of both Zn and Co are resolved (Fig. 3b for K-shell peak of Co). The peak intensities of both Si and Ca vary from one sample to another and disappear for 14 at. % films. This variation is assigned to different thicknesses of Co–ZnO films. The spectra are analyzed using Genesis Software, by considering only Zn, O and Co peaks (Table 2). The variation of the thickness of the films is due to the change of Zn and O content on one hand and the influence of oxygen that exists in the substrates on the other hand. The stoichiometry of the films is measured from Co and Zn signals. Let us define "*r*" as the ratio of the EDAX signals of Zn and Co and assume stoichiometric films of the form $Zn_{1-x}Co_xO$, with the Co atomic content x can be calculated as: $x = r/(1+r)$. Figure 4a, b shows the change of the ratio in EDX signal of Co/Zn ratio and Co atomic content, both plotted as function of the "expected" Co content from the deposition. Doping with Co is effective as long as the Co content does not exceed 14 at. %. At high Co concentration, the doping is ineffective and EDAX signal shows a discrepancy between the expected and measured atomic content of Co indicating that the limit of solubility of Co into ZnO solid solution is reached.

Table 2 Chemical composition of oxides from EDX spectra (atomic content %): expected composition vs. measured one

Films/element	O (K)	Zn (K and L)	Co (K and L)
$Zn_{0.99}Co_{0.01}O$	49.1	48.5	2.4
$Zn_{0.97}Co_{0.03}O$	38.6	59.7	1.7
$Zn_{0.95}Co_{0.05}O$	49.1	48.5	2.4
$Zn_{0.91}Co_{0.09}O$	43.3	52.8	3.9
$Zn_{0.86}Co_{0.14}O$	34.3	57.5	8.2
$Zn_{0.82}Co_{0.18}O$	45.4	49.1	5.5
$Zn_{0.78}Co_{0.22}O$	44.0	49.5	6.5

3.2 Optical properties

Transmittance spectra of $Zn_{1-x}Co_xO$ films are taken at room temperature to study their optical properties. They show the characteristic Co^{2+} absorptions in the visible and near-infrared spectral region at the wavelengths of 565, 611, 657, 1297, 1410 and 1648 nm. The first three peaks are the predominant absorptions. The dopant ion (Co^{2+}) transforms the colorless host lattice (ZnO) into green.

The solid curves in Figs. 5 and 6 correspond to the curve fitting and the symbols represent the experimental data. The figures reveal a reasonably good fitting to the experimental data, the values of d, E_g, E_d, E_0, rms, M^{-1}, M^{-3}, and n_∞ extracted by fitting [29] the experimental data are listed in Table 3. The decrease of energy value from 3.26 eV (pure ZnO) to 3.00 eV ($Zn_{0.78}Co_{0.22}O$) appears to originate from active transitions involving 3*d* levels in Co^{2+} ions and strong *sp–d* exchange interactions between the itinerant '*sp*' carriers (band electrons) and the localized '*d*' electrons of the dopant [35, 36].

Figure 7 presents the calculated refractive indices [29] of ZnO and $Zn_{1-x}Co_xO$ films. It is observed that the values of refractive indices at 598 nm of the ZnO, $Zn_{0.95}Co_{0.05}O$ and $Zn_{0.78}Co_{0.22}O$ films are equal to 1.77, 1.96 and 2.16, respectively.

The notion of Urbach parameter (E_{Urb}) is defined to characterize the disorder. It is possible to estimate the existing disorder in the layers by studying the variations

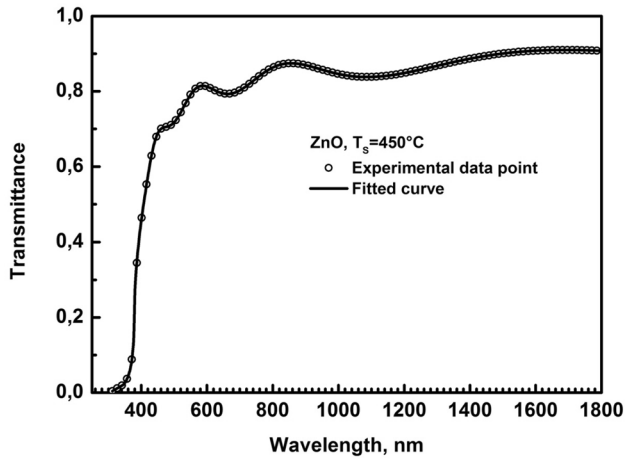

Fig. 5 Transmission spectrum of ZnO films is presented as a reference. Measured (full circles) and calculated (solid lines) transmittance spectra of films

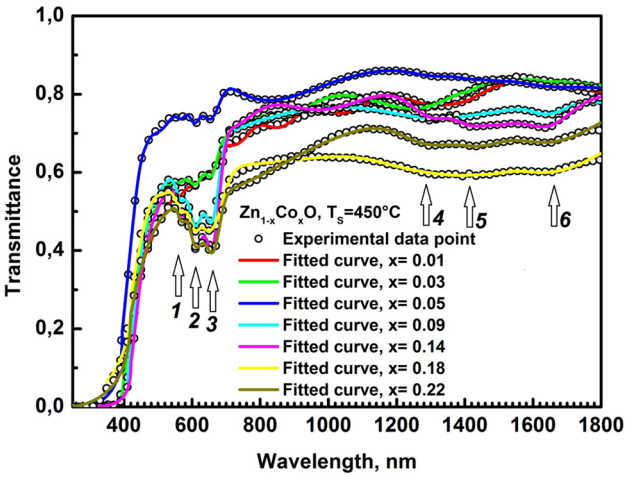

Fig. 6 Transmission spectra of $Zn_{1-x}Co_xO$ films deposited on glass substrate at 450 °C. Measured (full circles) and calculated (solid lines) transmittance spectra of films

of the absorption coefficient. Indeed, the absorption coefficient can be expressed by the equation [37]:

$$\alpha = \alpha_0 \exp\left(\frac{h\upsilon}{E_{\mathrm{Urb}}}\right) \qquad h\upsilon \prec E_{\mathrm{g}}. \tag{1}$$

All the experimental results for the variation of the optical bandgap of the thin layers and disorders as function of cobalt contents are shown in Fig. 8. It is observed that the bandgap decreases with increasing cobalt content. Therefore, the addition of Co increases the concentration of localized states in the thin film leading to the decrease of the bandgap.

Table 3 Dispersion parameters of the films extracted by fitting the experimental data

	Thickness (nm)	E_g (eV)	E_d (eV)	E_0 (eV)	n at 598 (nm)	n_∞	M^{-1}	$M^{-3}, \times 10^{-2}$ (eV)$^{-2}$	σ (nm)	Porosity (%)
ZnO	486	3.258	11.334	6.018	1.771	1.698	1.883	5.200	38	17.0
$Zn_{0.99}Co_{0.01}O$	1350	3.177	12.373	6.198	1.802	1.731	1.996	5.196	128	14.1
$Zn_{0.97}Co_{0.03}O$	846	3.097	13.478	6.185	1.859	1.783	2.179	5.696	130	09.7
$Zn_{0.95}Co_{0.05}O$	421	3.050	13.422	5.635	1.940	1.839	2.382	7.501	95	03.8
$Zn_{0.91}Co_{0.09}O$	463	3.075	11.621	6.061	1.781	1.708	1.917	5.219	40	15.7
$Zn_{0.86}Co_{0.14}O$	722	2.993	11.872	6.192	1.778	1.708	1.917	5.000	96	16.0
$Zn_{0.82}Co_{0.18}O$	396	3.023	19.290	5.947	2.166	2.060	3.243	9.171	74	–
$Zn_{0.78}Co_{0.22}O$	395	3.009	19.706	6.037	2.169	2.065	3.264	8.956	78	–

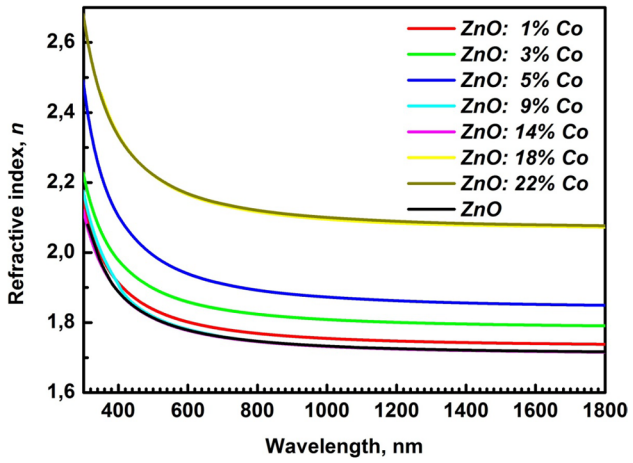

Fig. 7 Refractive index of $Zn_{1-x}Co_xO$ films

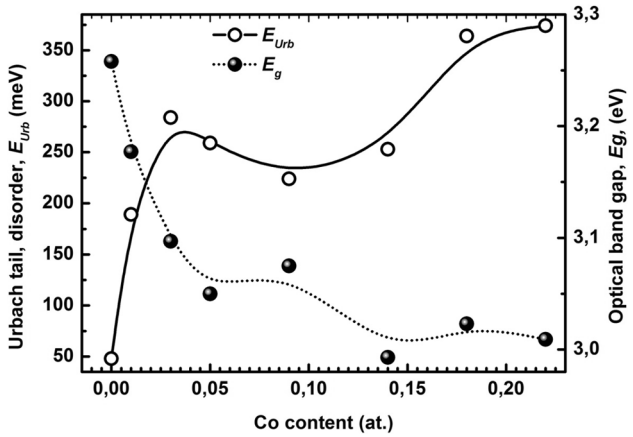

Fig. 8 Doping result and the variation of the bandgap and Urbach energy for different Co content

3.3 Photoluminescence spectroscopy

PL spectra depend on the stoichiometry and the microstructure of the films. ZnO is nonstoichiometric oxide containing oxygen vacancy (V_O) and reduced interstitial zinc species (Zn_i). In this work, the rapid evaporation–oxidation process, V_O should be generated because of partially incomplete oxidation and crystalline. Doping of Co^{2+} on ZnO may create defects in the film, which may provide non-radiative pathways to limit the radiative efficiency of the films.

Figure 9 shows the photoluminescence spectra of ZnO and $Zn_{1-x}Co_xO$ [with $x=5\%$, 9%, 14%, and 18%] which shows the presence of three emission bands at around 421 nm (2.94 eV), 485 nm (2.55 eV) and 528 nm (2.34 eV) for pure ZnO with a shift in the violet emission peak (421 nm) to 442 nm (2.80 eV) for the Co-doped films. Violet emission from ZnO at around 3.0 eV has been previously

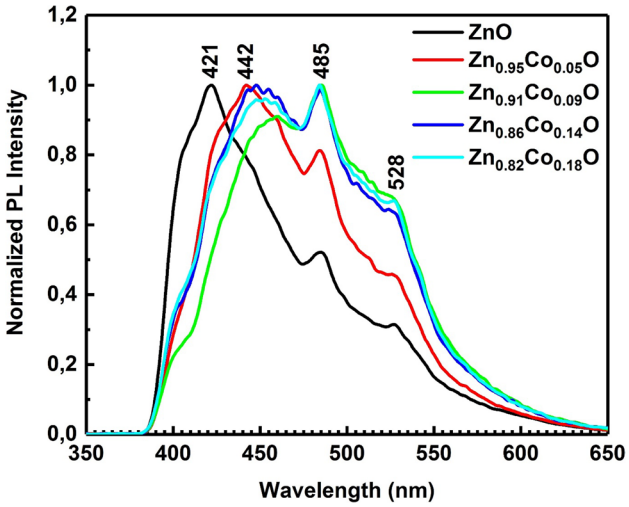

Fig. 9 PL spectra of ZnO and $Zn_{1-x}Co_xO$ ($x=5\%$, 9%, 14 and 18%) thin films measured at room temperature

reported from a sample prepared in an oxygen-deficient condition [38]. The oxygen vacancies of ZnO can produce two defect donor levels, the deep level at 1.3–1.6 eV and the shallow level at 0.3–0.5 eV below the conduction band [39]. The energy difference between this latter level and the valence band is 2.8 eV, which is consistent with the photon energy of the blue emission observed in this study. The other two peaks in the visible region are due to the presence of structural defects such as oxygen vacancies (V_O) and zinc interstitials (Zn_i) [40, 41].

It was found that the PL emission intensity of ZnO was obviously affected by the doping of Co. This phenomenon might originate from the interaction between the Co doping and native defects such as oxygen vacancies (V_O) [42].

3.4 Magnetic properties

The pure ZnO sample exhibits diamagnetic behaviour which agree with previous researches trend [43, 44]. However, the Co-doped ZnO thin films exhibits S-shape *M–H* curve, indicating ferromagnetic properties. It can be caused by defects in the ZnO after doping metal ion [45, 46]. In Co-doped ZnO thin films, the doping of Co^{2+} yields increased magnetization values because Co^{2+} in the half-filled 3*d* shell has five spins, which normally gives a maximum dipole moment value of 3 μ_B/Co ion [47].

Figure 10 displays room temperature magnetization-field (*M–H*) curves of ZnO and $Zn_{1-x}Co_xO$ ($x=5\%$ and 14%) thin films. The inset presents the *M–H* curves of $Zn_{1-x}Co_xO$ ($x=5\%$ and 14%) films when the diamagnetic contribution from ZnO has been subtracted. Diamagnetic contribution of glass substrate and sample holder has been subtracted from the recorded data. The values for magnetization (emu/cm^3)

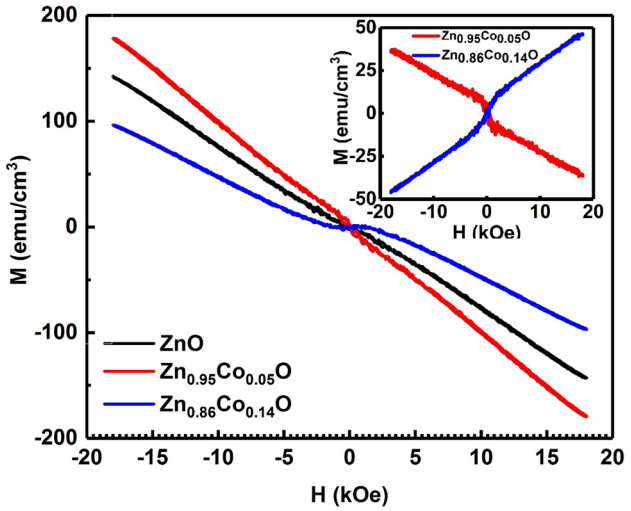

Fig. 10 Magnetization versus magnetic field (*M–H*) curves at room temperature for ZnO and $Zn_{1-x}Co_xO$ ($x=5\%$ and 14%) thin films. The inset presents the *M–H* curves of $Zn_{1-x}Co_xO$ ($x=5\%$ and 14%) films when the diamagnetic contribution from ZnO has been subtracted

were calculated against the sample volume, estimated from the measured surface area of the sample and the film thickness. It can be observed from Fig. 10 that the magnetic properties of ZnO thin films are strongly influenced by the doping concentration. The S-shaped form of the hysteresis loop indicates that the $Zn_{0.86}Co_{0.14}O$ films show a weak ferromagnetic behaviour, in the low field range, alongside with diamagnetic component, whereas the ZnO and $Zn_{0.95}Co_{0.05}O$ films reveal a dominant diamagnetic component. The interaction between the Co doping and native defect such as oxygen vacancies (PL emission peak centered at around 442 nm) is found to be the main reason for room temperature ferromagnetism in the Co-doped ZnO films with the support of the results obtained from the photoluminescence studies.

The concentration of cobalt cations N_{Co} for a 14 at. % doping level in the films can be calculated as:

$$N_{Co} = \frac{\rho_{film} N_{Av}}{M} \times 0.14, \tag{2}$$

where N_{Av} is the Avogadro constant, M is molar mass and ρ_{film} is mass density of the film. The average mass density of the film ρ_{film} is related to the porosity (P) and bulk density (ρ_{bulk}) of ZnO through the following equation:

$$\rho_{film} = \rho_{bulk}(1 - P). \tag{3}$$

The porosity P is calculated from optical constants using the Lorentz–Lorenz equation [48]:

$$P = 1 - \frac{(n_{film}^2 - 1)\,(n_{bulk}^2 + 2)}{(n_{film}^2 + 2)\,(n_{bulk}^2 - 1)}, \tag{4}$$

where n_{film} (1.778 at 598 nm) is the refractive indices of the porous $Zn_{0.86}Co_{0.14}O$ films and n_{bulk} is the refractive indices of the ZnO bulk which is 1.996 at 598 nm.

We determined $P=0.16$, $\rho_{film}=4.71$ g cm^{-3} against the bulk density $\rho_{bulk}=5.61$ g cm^{-3} and one gets the value of $N_{Co}=4.88\times10^{21}$ cm^{-3}.

The saturation magnetization is not observed up to the maximum applied field of 18 kOe, as shown in the inset of Fig. 10. The magnetization values observed at 18 kOe are 46.43 emu/cm^3, namely, $1.02\mu_B$/Co (1 emu $=1.0783\times10^{20}$ μ_B).

4 Conclusion

X-ray diffraction analysis using the Rietveld method shows that the as-deposited ZnO and $Zn_{1-x}Co_xO$ ($x=0.01$–0.22) films are pure of single wurtzite phase. The lattice parameter "a" increases with Co content while "c" is affected, thereby the volume of unit cell increases with increasing Co. The Co doping into ZnO solid solution is found to influence considerably the film morphology, the grain size, and the stoichiometry of the oxide. The doping effectiveness is revealed by EDAX analysis of the chemical composition of the films and it shows good agreement between the expected and measured Co atomic content. The presence of high concentrations of localized states in the thin films is responsible for the reduction in the width of optical bandgap. On the other hand, all the photoluminescence spectra have the same comportment. They show three emission peaks with different intensities located in the visible region. The interaction between the Co doping and native defect such as oxygen vacancies is found to be the main reason for room temperature ferromagnetism in the Co-doped ZnO films with the support of the results obtained from the photoluminescence studies.

Acknowledgements The authors would like to thank the National Project Research (PNR) and LASPI^{2}A Laboratory of Khenchela University (Algeria) for their financial support of this research project. The authors thank Dr. Ali Hafs for VSM measurements, Laboratoire de Physicochimie des Matériaux (LPCM), El Tarf University, 36000 El Tarf, Algeria.

References

1. S. Oktik, Low cost non-vacuum techniques for the preparation of thin/thick films for photovoltaic applications. Prog. Cryst. Growth Charact. **17**, 171–240 (1988)
2. K. Bouzid, A. Djelloul, N. Bouzid, J. Bougdira, Electrical resistivity and photoluminescence of zinc oxide films prepared by ultrasonic spray pyrolysis. Phys. Status Solid. A. **206**, 106–115 (2009)
3. A. Janotti, ChG Van de Walle, Fundamentals of zinc oxide as a semiconductor. Rep. Prog. Phys. **72**, 126501 (2009)

4. K. Ellmer, A. Klein, B. Rech (eds.), *Transparent Conductive Zinc Oxide-Basics and Applications in Thin Film Solar Cells*. (Series: Springer Series in Materials Science, Berlin, 2008), p. 104
5. H.M. Yang, S. Nie, Preparation and characterization of Co-doped ZnO nanomaterials. Mater. Chem. Phys. **114**, 279–282 (2009)
6. M. Yang, Z.X. Guo, K.H. Qiu, J.P. Long, G.F. Yin, D.G. Guan, S.T. Liu, S.J. Zhou, Synthesis and characterization of Mn-doped ZnO column arrays. Appl. Surf. Sci. **256**, 4201–4205 (2010)
7. H. Saal, T. Bredow, M. Binnewies, Band gap engineering of ZnO via doping with manganese: effect of Mn clustering. Phys. Chem. Chem. Phys. **11**, 3201–3209 (2009)
8. G.M. Kumar, P. Ilanchezhiyan, J. Kawakita, M. Subramanian, R. Jayavel, Magnetic and optical property studies on controlled low-temperature fabricated one-dimensional Cr doped ZnO nanorods. Cryst. Eng. Commun. **12**, 1887–1892 (2010)
9. S. Fabbiyola, L.J. Kennedy, U. Aruldoss, M. Bououdina, A.A. Dakhel, J. Judith Vijaya, Synthesis of Co-doped ZnO nanoparticles via co-precipitation: structural, optical and magnetic properties. Powder Technol. **286**, 757–765 (2015)
10. T. Dietl, H. Ohno, F. Matsukura, J. Cibert, D. Ferrand, Zener model description of ferromagnetism in zinc-blende magnetic semiconductors. Science **287**, 1019–1022 (2000)
11. Y.X. Wang, X. Ding, Y. Cheng, Y.J. Zhang, L.L. Yang, H.L. Liu, H.G. Fan, Y. Liu, J.H. Yang, Properties of Co-doped ZnO films prepared by electrochemical deposition. Cryst. Res. Technol. **44**(5), 517–520 (2009)
12. C. Song, F. Zeng, K.W. Geng, X.B. Wang, Y.X. Shen, F. Pan, The magnetic properties of Co-doped ZnO diluted magnetic insulator films prepared by direct current reactive magnetron co-sputtering. J. Magn. Magn. Mater. **309**, 25–30 (2007)
13. A. Zukova, A. Teiserskis, S. van Dijken, Y.K. Gun'ko, V. Kazlauskiene, Giant moment and magnetic anisotropy in Co-doped ZnO films grown by pulse-injection metal organic chemical vapor deposition. Appl. Phys. Lett. **89**, 232503–232505 (2006)
14. H. Matsui, H. Tabata, Simultaneous control of growth mode and ferromagnetic ordering in Co-doped ZnO layers with Zn polarity. Phys. Rev. B. **75**, 014438–014447 (2007)
15. A. Sivagamasundari, R. Pugaze, S. Chandrasekar, S. Rajagopan, R. Kannan, Absence of free carrier and paramagnetism in cobalt-doped ZnO nanoparticles synthesized at low temperature using citrate sol–gel route. Appl. Nanosci. **3**, 383–388 (2013)
16. G. Iqbal, S. Faisal, S. Khan, D.F. Shams, A. Nadhman, Photo-inactivation and efflux pump inhibition of methicillin resistant *Staphylococcus aureus* using thiolated cobalt doped ZnO nanoparticles. J. Photochem. Photobiol. B Biol. **192**, 141–146 (2019)
17. H.S. Sindhu, S. D. Kulkarni, R.J. Choudhary, P.D. Babu, B.V. Rajendra, Influence of cobalt doping on structure, optical and magnetic properties of spray pyrolysed nano structured ZnO films. Phys. B: Phys. Condens. Matter. https://doi.org/10.1016/j.physb.2019.07.034
18. M. Ivill, S.J. Pearton, S. Rawal, L. Leu, P. Sadik, R. Das, A.F. Hebard, M. Chisholm, J.D. Budai, D.P. Norton, Structure and magnetism of cobalt doped ZnO thin films. New J. Phys. **10**, 065002 (2008)
19. N.K. Tarwal, K.V. Gurav, T. PremKumar, Y.K. Jeong, H.S. Shim, I.Y. Kim, J.H. Kim, J.H. Jang, P.S. Patil, Structure, X-ray photoelectron spectroscopy, and photoluminescence investigations of the spray deposited cobalt doped ZnO thin films. J. Anal. Appl. Pyrolysis **106**, 26–32 (2014)
20. S. Karamat, R.S. Rawat, T.L. Tan, P. Lee, R. Chen, H.D. Sun, W. Zhou, Ferromagnetism in ZnCoO thin films deposited by PLD. Appl. Phys. A **101**, 717–722 (2010)
21. C.B. Fitzgerald, M. Venkatesan, J.G. Lunney, L.S. Dorneles, J.M.D. Coey, Cobalt-doped ZnO—a room temperature dilute magnetic semiconductor. Appl. Surf. Sci. **247**, 493–496 (2005)
22. A. Dinia, G. Schmerber, C. Mény, V. Pierron-Bohnes, E. Beaurepaire, Room- temperature ferromagnetism in $Zn_{1-x}Co_xOZn_{1-x}Co_xO$ magnetic semiconductors prepared by sputtering. J. Appl. Phys. **97**, 123908 (2005)
23. G. Lawes, A.S. Risbud, A.P. Ramirez, R. Seshadri, Absence of ferromagnetism in Co and Mn substituted polycrystalline ZnO. Phys. Rev. B. **71**, 045201 (2005)
24. J.H. Park, M.G. Kim, H.M. Jang, S. Ryu, Y.M. Kim, Co-metal clustering as the origin of ferromagnetism in Co-doped ZnO thin films. Appl. Phys. Lett. **84**, 1338 (2004)
25. J.H. Kim, H. Kim, D. Kim, Y.E. Ihm, W.K. Choo, Magnetic properties of epitaxially grown semiconducting $Zn_{1-x}Co_xOZn_{1-x}Co_xO$ thin films by pulsed laser deposition. J. Appl. Phys. **92**, 6066 (2002)
26. Y.Z. Peng, T. Liew, W.D. Song, C.W. An, K.L. Teo, T.C. Chong, Structural and optical properties of Co-doped ZnO thin films. J. Supercond. **18**, 97–103 (2005)
27. R. Siddheswaran, R. Medlín, C.E. Jeyanthi, S.G. Raj, R.V. Mangalaraja, Structural, morphological, optical and magnetic properties of RF sputtered Co doped ZnO diluted magnetic semiconductor for spintronic applications. Appl. Phys. A **9**, 125 (2019). https://doi.org/10.1007/s00339-019-2886-0
28. A. Aravind, K. Hasna, M.K. Jayaraj, M. Kumar, R. Chandra, Magnetic and Raman scattering studies of Co-doped ZnO thin films grown by pulsed laser deposition. Appl. Phys. A **115**(3), 843–849 (2014)
29. S. Roguai, A. Djelloul, C. Nouveau, T. Souier, A.A. Dakhel, M. Bououdina, Structure, microstructure and determination of optical constants from transmittance data of Co-doped $Zn_{0.90}Co_{0.05}M_{0.05}O$ (M = Al, Cu, Cd, Na) films. J. Alloys Compd. **599**, 150–158 (2014)
30. M. Bouloudenine, N. Viart, S. Colis, J. Kortus, A. Dinia, Antiferromagnetism in bulk $Zn_{1-x}Co_xO$ $Zn_{1-x}Co_xO$ magnetic semiconductors prepared by the coprecipitation technique. Appl. Phys. Lett. **87**, 052501 (2005)
31. X.C. Chen, J.P. Zhou, H.Y. Wang, P.S. Xu, G.Q. Pan, Chin. Phys. B. **20**, 9 (2011)
32. D. Bao, H. Gu, A. Kuang, Sol-gel-derived *c*-axis oriented ZnO thin films. Thin Solid Films **312**, 37–39 (1998)
33. S. Benramache, B. Benhaoua, Influence of substrate temperature and Cobalt concentration on structural and optical properties of ZnO thin films prepared by ultrasonic spray technique. Superlattices Microstruct. **52**, 807–815 (2012)
34. G. Vijayaprasath, R. Murugan, G. Ravi, T. Mahalingam, Y. Hayakawa, Characterization of dilute magnetic semiconducting transition metal doped ZnO thin films by a sol-gel spin coating method. Appl. Surf. Sci. **313**, 870–876 (2014)
35. P. Lommens, P.F. Smet, C.M. Donega, A. Meijerink, L. Piraux, S. Michotte, S.M. Tempfli, D. Poelman, Z. Hens, Photoluminescence properties of Co^{2+}-doped ZnO nanocrystals. J. Lumin. **118**, 245–250 (2006)
36. A.S. Pereira, A.O. Ankiewicz, W. Gehlhoff, A. Hoffmann, S. Pereira, T. Trindade, M. Jrundmann, M.C. Carmo, N.A. Sobolev, Surface modification of Co-doped ZnO nanocrystals and its effects on the magnetic properties. J. Appl. Phys. **103**, 07D140 (2008). https://doi.org/10.1063/1.2833300
37. F. Urbach, The long-wavelength edge of photographic sensitivity and electronic absorption of solids. APS J. Phys. Rev. **92**, 1324–1326 (1953)
38. B.J. Jin, S. Im, S.Y. Lee, Violet and UV luminescence emitted from ZnO thin films grown on sapphire by pulsed laser deposition. Thin Solid Films **366**, 107–110 (2000)
39. D.H. Zhang, Z.Y. Xue, Q.P. Wang, The mechanisms of blue emission from ZnO films deposited on glass substrate by r.f. magnetron sputtering. J. Phys. D. **35**, 2837 (2002)

40. A. Kaphle, P. Hari, Characterization of aluminium doped nanostructured ZnO/p-Si heterojunctions. Int. J. Eng. Sci. (IJES) **5**, 41–51 (2016)
41. U. Godavarti, V.D. Mote, M.V. Ramana Reddy, P. Nagaraju, Y. VijayKumar, K. T. Dasari, M. P. Dasari, Precipitated cobalt doped ZnO nanoparticles with enhanced low temperature xylene sensing properties. Phys. B Phys. Condens. Matter. **533**, 151–160 (2019). https://doi.org/10.1016/j.physb.2018.10.034
42. U. Philipose, S.V. Nair, S. Trudel, C.F. Souza, S. Aouba, R.H. Hill, H.E. Ruda, High- temperature ferromagnetism in Mn-doped ZnO nanowires. Appl. Phys. Lett. **88**, 263101 (2006)
43. L. Xu, H. Zhang, K. Shen, M. Xu, Q. Xu, Room temperature ferromagnetism in Co-doped ZnO prepared by microemulsion. J. Supercond. Nov. Magn. **25**, 1951–1956 (2012)
44. M. Shatnawi, A.M. Alsmadi, I. Bsoul, B. Salameh, G.A. Alna'Washi, F. Al-Dweri, F. El Akkad, Magnetic and optical properties of Co-doped ZnO nanocrystalline particles. J Alloys. Compd. **655**, 244–252 (2016)
45. Z. Xiong, X.C. Liu, S.Y. Zhuo, J.H. Yang, E.W. Shi, W.S. Yan, Oxygen enhanced ferromagnetism in Cr-doped ZnO films. Appl. Phys. Lett. **99**, 052513 (2011)
46. J.A. Wibowo, N.F. Djaja, R. Saleh, Cu- and Ni-doping effect on structure and magnetic properties of Fe-doped ZnO nanoparticles. Adv. Mater. Phys. Chem. **3**, 48–57 (2013)
47. J.R. Neal, A.J. Behan, R.M. Ibrahim, H.J. Blythe, M. Ziese, A.M. Fox, G.A. Gehring, Room-temperature magneto-optics of ferromagnetic transition-metal-doped ZnO thin films. Phys. Rev. Lett. **96**, 197208–197212 (2006)
48. M. R. Baklanov, K. P. Mogilnikov, V. G. Polovinkin, F. N. Dultsev, Determination of pore size distribution in thin films by ellipsometric porosimetry. J. Vac. Sci. Technol. B. **18**, 1385–1391(2000).